Reports

Oxidation Fronts in Pelagic Sediments: Diagenetic Formation of Metal-Rich Layers

T. R. S. WILSON, J. THOMSON, D. J. HYDES, S. COLLEY, F. CULKIN, J. SØRENSEN

The periodic deposition of distal turbidites at a site on the Madeira Abyssal Plain causes the development of a nonsteady-state diagenetic system in which an oxidation front migrates downward into the sediment. Data presented here show that iron, manganese, and particulate organic carbon are oxidized at this front by oxidants (molecular oxygen and nitrate) diffusing from above. A numerical model of systems of this type predicts the formation of iron-rich layers under certain nonsteady-state conditions. The layers predicted by the model are closely comparable in thickness and general morphology to iron-rich layers found in certain ocean sediments, the origin of which has been until now unexplained.

RECENT STUDIES (*1*, *2*) HAVE shown that under certain circumstances oxidation fronts may develop and progress downward into deep-ocean sediments. This report deals with the distribution of iron at such fronts and shows that under certain conditions nonsteady-state diagenesis produces iron-rich layers similar to those that have been observed in sediments, particularly at depths close to the most recent transition from glacial to interglacial conditions (*3*–*7*).

A "progressive oxidation front" mechanism, in which the various stages of the redox succession that occur during organic diagenesis (*7*–*9*) may be localized in a relatively thin zone within the sediment, has been shown (*2*) to be responsible for the observed pattern of diagenetic behavior at R.R.S. *Discovery* station 10554. This process was further investigated in sediments from an adjacent area obtained on *Discovery* cruise 149. The data set from box core 11137 on the Madeira Abyssal Plain (Fig. 1) is typical of several box cores obtained from this turbidite. Although the active turbidite layer at this site has a markedly lower content of organic carbon than that at station 10554, a similar sharp redox drop occurs at the front in an otherwise vertically homogeneous turbidite. The Fe^{2+} distribution close to such fronts has not been previously reported; the results presented here (Fig. 1) show that the pore-water concentrations of both Fe^{2+} and Mn^{2+} increase with depth below the oxidation front. Thus, there is a transition from O_2-containing to Fe^{2+}-containing pore water within a very small vertical interval. The sulfate levels in the pore waters indicate that sulfate reduction is not active in these sediments.

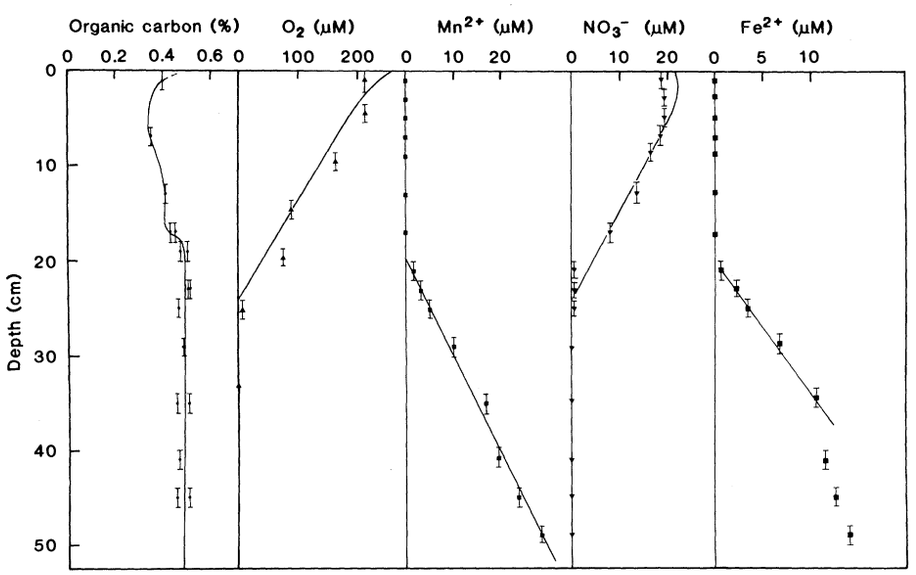

Fig. 1. Pore-water and solid-phase organic carbon data for box core 11137 3BX. Lines drawn for Mn^{2+} and Fe^{2+} represent fixed gradients used in the model calculations. Curves for O_2 and NO_3^- are calculated from the model equations (Table 1B) and the data given in Table 2 for the Madeira Abyssal Plain. The color change occurred at 22 cm in this core. Bars indicate sample depth intervals.

A progressive oxidation front phenomenon may be initiated by any relatively sudden change in sedimentary conditions that causes the actual oxidized sediment surface layer thickness to become smaller than the equilibrium steady-state layer thickness. This might occur, for instance, as a result of the deposition of an organic-rich turbidite, a decrease in organic sedimentation rate, or an increase in the rate of supply of O_2 via bottom water. Such events may be linked to climatic changes (*10*–*12*). The resultant front then deepens the upper oxidized zone by propagating downward at a rate determined by the reducing capacity of the sediment (organic carbon and reduced inorganic species) and the instantaneous balance between the diffusive fluxes of oxidants (O_2 and NO_3^-) and reductants (Mn^{2+} and Fe^{2+}). As the diffusion distance increases, the downward migration rate of the front drops. When the oxidative flux becomes equal to the reductive flux, no further reaction of particulate organic carbon can occur and the downward penetration of the reaction front ("burn-down") ceases. With further accumulation at the sediment-water interface, the point of zero O_2 and NO_3^- concentrations then moves upward to maintain a constant distance from this interface, as steady-state conditions are established with the new accumulation regime (*13*).

A numerical model (*14*), which includes the processes of (i) bioturbation, (ii) surficial respiration and nitrification, (iii) denitrification, and (iv) diffusion of O_2, NO_3^-, Fe^{2+}, and Mn^{2+}, has been developed to predict the rate of burn-down of the redox front. The relevant equations are shown in Table 1. This model may be used to estimate the time that has elapsed since the deposition of the most recent turbidite. Its application to the conditions found at station 11137 is summarized in Table 2. In the model it is assumed that, apart from the downward migration of the front, the observed conditions within the sediment have obtained continuously since the deposition event. Supporting evidence for a relatively

T. R. S. Wilson, J. Thomson, D. J. Hydes, S. Colley, F. Culkin, Institute of Oceanographic Sciences, Brook Road, Wormley, Godalming, Surrey, GU8 5UB, United Kingdom.
J. Sørensen, Department of Ecology and Genetics, University of Aarhus, Ny Munkegade, DK-8000, Aarhus C, Denmark.

recent deposition event (217 years before the present) is provided by the observed lack of detectable overlying pelagic sediment and the characteristic benthic faunal distribution observed in bottom photographs (*15*).

The model predictions of the depositional history of iron and manganese over longer periods of time are of particular interest. The exponentially slowing front "hovers" close to its maximum depth of penetration for a considerable period. During this time, Mn^{2+} and Fe^{2+}, arriving at the front by diffusion, are oxidized and precipitate in a narrow depth interval, which consequently becomes considerably enriched in these elements. At the Madeira Abyssal Plain site, the arrival of turbidites is apparently too frequent, and the Fe^{2+} flux is too low, to permit the process to develop to this degree of maturity. However, layers rich in iron and manganese have been reported for other areas such as the western equatorial Atlantic (*3, 4*), the Gulf of Mexico (*5, 6*), the Coral Sea, the Caribbean Sea, the Bahama Outer Ridge, the Mediterranean Sea, the Sierra Leone Rise, and the Ganges Abyssal Fan (*4*). These layers frequently, but not always, exhibit millimeter-scale laminations. Parallel enrichments with manganese, cobalt, and nickel have also been reported (*3, 5*). The layers are typically located at or just below the Pleistocene-Holocene transition zone. Sediments below this zone are typically richer in clay and organic carbon and poorer in calcite than those above; frequently, a marked drop in accumulation rate occurs (*3, 12, 16*). Such changes in the sedimentation regime imply a deepening of the equilibrium oxygenated layer (*13*). A sudden transition of this type would be capable of initiating the formation of a progressive diagenetic front.

Various mechanisms have been proposed to account for the formation of iron-rich layers. Watson and Angino (*5*) suggested a mechanism involving scavenging from the overlying seawater. McGeary and Damuth (*4*) proposed that pore solutions containing iron(II) were expelled from the sediment by compaction so that the iron-rich layer formed at the sediment-water interface. Normal compaction does not expel pore fluid in this way, although in special circumstances diffusion may supply iron to be precipitated at the sediment-water interface (*17*). However, any proposed mechanism that requires that these iron-rich layers formed at the interface must account for their subsequent preservation in spite of the disruptive activities of benthic organisms. In oxygenated bottom-water conditions, the absence of bioturbation for the required burial period of several thousand years is most unlikely. Richardson (*3*) recognized that the layers are produced within the sediment by the upward diffusion of Fe(II), but she did not satisfactorily explain the sharp depth localization of the metal-rich sediment. The reaction front mechanism proposed here explains this localization in a simple and quantitative manner.

Figure 2 compares the field results of Richardson (*3*) with iron profiles predicted by the numerical model. Because Richardson's cores were sampled at coarse depth intervals, generally 10 cm, we used the qualitative core descriptions, which include visual estimates of the thickness of the iron-rich layer, to interpolate between the depths for which analytical data are given (*3*).

Figure 2 also illustrates the sensitivity of the model predictions to variation of the input parameters over the likely range existing at Richardson's stations. The observed narrow depth interval of the highest enrichments is in good agreement with the model predictions over virtually the whole range of input conditions. Factors exerting a direct influence on the fluxes of oxidants and reductants are the most critical. Bioturbation in the overlying layers, and possibly bottom-water changes, are likely to cause inconstancy in the oxidant fluxes. Model experiments in which the O_2 flux was made to vary by 10 percent in a system close to the balance point produced layers containing several overlapping peaks, similar to the natural laminated structures.

Richardson (*3*) observed that the solid-phase manganese peak is either coincident with the iron peak or is located a few centimeters above it. Coincidence of the two peaks implies that the burn-down process is still slowly oxidizing sediment organic carbon. Subsequently, as sedimentation continues, manganese appears to be remobilized in preference to iron for kinetic or thermodynamic reasons and tracks the retreating O_2 profile upward. This process represents the first step toward the establishment of a steady-state regime (*13*). Richardson (*3*) found that cobalt and nickel did not always correlate with manganese, particularly in profiles in which manganese remobilization has begun; this may reflect fractionation effects associated with differential mobilization of the various transition metals.

Our model shows that sharp layers can develop well below the zone of active bioturbation, typically a decimeter thick (*18,*

Table 1. Equations used in the numerical model. Redfield stoichiometric relationships (A) for the breakdown of particulate organic carbon compounds by oxidation and by denitrification; NO_3^-, produced by the oxidative breakdown process (Eq. 1), supplements the diffusive NO_3^- supply to the reaction front. The assumption that goethite and hausmannite are directly produced at the reaction front (Eqs. 3 and 4) is a simplification introduced to avoid overelaboration of the model. Equations (B) derived analytically (*2*) by the use of steady-state assumptions. Since the rate of increase of the oxidized layer thickness is always small with respect to the rate at which diffusive equilibrium can be established (*20*), the quasi–steady-state assumption used in the present model is valid. Most symbols are explained in Table 2; Z_L is the instantaneous redox front depth, P is the instantaneous slope of the linear portion of the O_2 profile, and F is the corresponding slope of the linear portion of the NO_3^- profile; β is estimated from the surficial layer depth (Z_1) by means of the expression $\beta = -\ln(0.01)/Z_1$ (*2*).

(A) Stoichiometric assumptions incorporated into the numerical model:

$$138\ O_2 + (CH_2O)_{106}(NH_3)_{16}H_3PO_4 + 18\ HCO_3^- = 124\ CO_2 + 16\ NO_3^- + HPO_4^{2-} + 140\ H_2O \quad (1)$$

$$94.4\ NO_3^- + (CH_2O)_{106}(NH_3)_{16}H_3PO_4 = 13.6\ CO_2 + 92.4\ HCO_3^- + 55.2\ N_2 + 84.8\ H_2O + HPO_4^{2-} \quad (2)$$

$$4\ Fe^{2+} + 3\ O_2 + 2\ H_2O = 4\ FeOOH\ (goethite) \quad (3)$$

$$3\ Mn^{2+} + 2\ O_2 = Mn_3O_4\ (hausmannite) \quad (4)$$

(B) Analytic equations used to calculate O_2 and NO_3^- profiles:

$$[O_2] = \frac{138}{106}\frac{D_B}{\varphi D_0}[\hat{C}]_0 e^{-\beta Z} + (Z - Z_L)P \quad (5)$$

$$[NO_3^-] = -\frac{16}{106}\frac{D_B}{\varphi D_N}[\hat{C}]_0 e^{-\beta Z} + (Z - Z_L)F \quad (6)$$

Expressions for the flux of O_2 and NO_3^- to the redox front:

$$\text{Flux of } O_2 = -D_0P = \frac{D_0}{Z_L}\left([O_2]_0 - \frac{138}{106}\frac{D_B}{\varphi D_0}[\hat{C}]_0\right) \quad (7)$$

$$\text{Flux of } NO_3^- = -D_NF = \frac{D_N}{Z_L}\left([NO_3^-]_0 + \frac{16}{106}\frac{D_B}{\varphi D_N}[\hat{C}]_0\right) \quad (8)$$

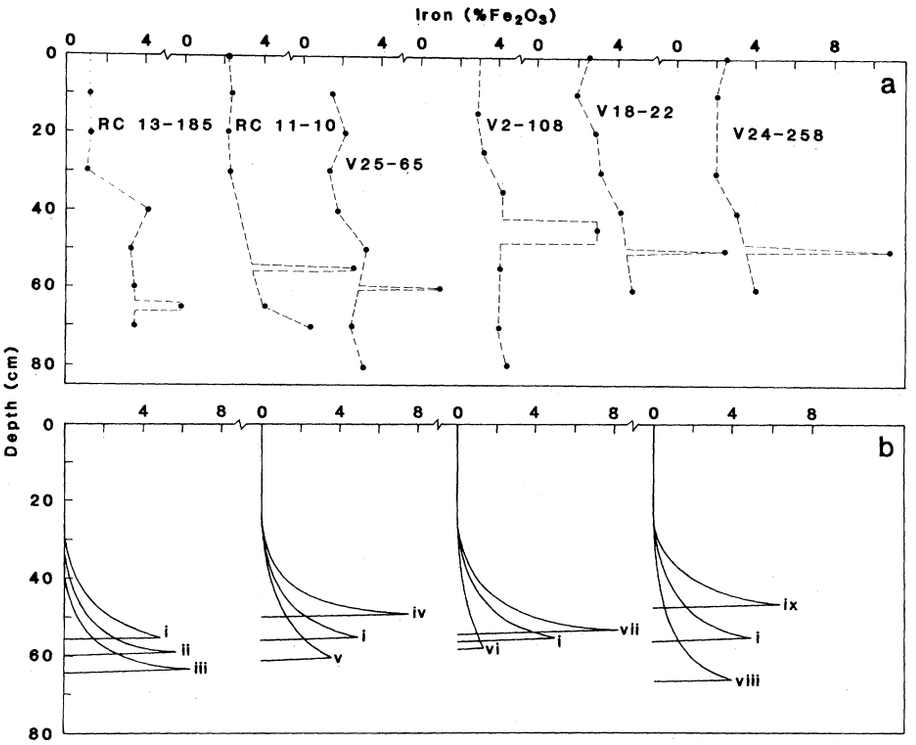

Fig. 2. (a) Field data of Richardson (*3*). Dashed lines join nonpeak points; the peaks are then interpolated on the basis of visual information reported in Richardson's table 4.1. The core data, derived from samples 1 or 2 cm thick, probably underestimate the maximum iron enrichments. (b) Model results obtained (i) on the basis of the use of the input data given in Table 2. Other runs mirror (i) except as follows: (ii) the accumulation rate is 3 cm per 10^3 years; (iii) the accumulation rate is 3.5 cm per 10^3 years; (iv) bottom water $[O_2]$ equals 200 μmol liter^{-1}; (v) $[O_2]$ equals 240 μmol liter^{-1}; (vi) iron flux is 3×10^{-15} μmol cm^{-2} sec^{-1}; (vii) iron flux is 9×10^{-15} μmol cm^{-2} sec^{-1}; (viii) labile organic carbon is 0.25%; (ix) labile organic carbon is 1.0%. To facilitate comparison, we smoothed the model data by computing a running average of the iron content at the five depth-mesh points centered at the nominal depth point, degrading the vertical resolution of the model (0.2 cm) to correspond to that of the core data.

Table 2. Model input data. The surficial oxidation-zone data used throughout the model run for station 11137 were obtained by an empirical fit to the observed O_2 and NO_3^- profiles. Diffusion coefficients were taken from Li and Gregory (*21*). Base case data are listed for the western equatorial Atlantic model runs; the sensitivity of the model to input changes is illustrated in Fig. 2.

Parameter	Symbol in Table 1	Madeira Abyssal Plain (station 11137)	Western equatorial Atlantic (*3*)
Input data			
Model time step (years)		0.1	1.0
Concentration gradients			
Mn^{2+} ($\times 10^{-10}$ mol cm^{-4})		9.7	9.7
Fe^{2+} ($\times 10^{-10}$ mol cm^{-4})*		7.2	28.8
Diffusion coefficients			
O_2 ($\times 10^{-6}$ cm^2 sec^{-1})	D_0	8.3	8.3
NO_3^- ($\times 10^{-6}$ cm^2 sec^{-1})	D_N	6.6	6.6
Mn^{2+} ($\times 10^{-6}$ cm^2 sec^{-1})		2.3	2.3
Fe^{2+} ($\times 10^{-6}$ cm^2 sec^{-1})		2.4	2.4
Bottom-water O_2 ($\times 10^{-9}$ mol cm^{-3})	$[O_2]_0$	245	220
Bottom-water NO_3^- ($\times 10^{-9}$ mol cm^{-3})	$[NO_3^-]_0$	22.3	30
Sediment			
Surficial zone depth (cm)	Z_1	12	12
Surficial labile organic carbon (%)	$[\hat{C}]_0$	0.3	1.0
Accumulation rate ($\times 10^{-3}$ cm year^{-1})		1.0	2.5
Bioturbation coefficient ($\times 10^{-9}$ cm^2 sec^{-1})	D_B	2.18	2.18
Bulk dry density (g cm^{-3})		0.5	0.5
Porosity	φ	0.7	0.7
Initial bulk labile organic carbon (%)		0.1	0.5
Run time† ($\times 10^3$ years)			11.0
Maximum depth of oxidation front‡ (cm)		24	
Output data			
Run time (years)		217	
Depth of oxidation front (cm)			55.6
Maximum iron enrichment above front (% Fe_2O_3)		0.01	5.0
Maximum manganese enrichment above front (% Mn_3O_4)		0.02	2.1
Estimated present downward front velocity (cm year^{-1})		0.056	0.0007

*No pore-water data are available for western equatorial Atlantic stations; these values are assumed to be equal to the observed values for station 11137, except that the Fe^{2+} flux is assumed to be four times the station 11137 value. Bottom-water O_2 and NO_3^- values are estimated from GEOSECS data (*22*). †The change to high-O_2 bottom water is assumed to coincide with the end of the transition to Holocene conditions. ‡Observed zero O_2 depth (color change is 2 cm above this point), station 11137.

19), and explains how these layers are frequently, but not inevitably, made up of finer bands or laminations. It follows that the presence of diagenetic fine structure in sediments does not necessarily imply the absence of bioturbation during the formation period, since such structure can be produced below the depth of maximum bioturbation.

REFERENCES AND NOTES

1. S. Colley, J. Thomson, T. R. S. Wilson, N. C. Higgs, *Geochim. Cosmochim. Acta* **48**, 1223 (1984).
2. T. R. S. Wilson, J. Thomson, S. Colley, D. J. Hydes, N. C. Higgs, J. Sørensen, *ibid.* **49**, 811 (1985).
3. D. Richardson, thesis, Columbia University (1974).
4. D. F. R. McGeary and J. E. Damuth, *Geol. Soc. Am. Bull.* **84**, 1201 (1973).
5. J. A. Watson and E. E. Angino, *J. Sediment. Petrol.* **39**, 1412 (1969).
6. J. H. Trefry and B. J. Presley, in *Marine Pollutant Transfer*, H. L. Windom and R. A. Duce, Eds. (Lexington Books, Lexington, MA, 1976), pp. 39–76.
7. G. E. Claypool and I. R. Kaplan, in *Natural Gases in Marine Sediments*, I. R. Kaplan, Ed. (Plenum, New York, 1974), pp. 99–114.
8. P. N. Froelich *et al.*, *Geochim. Cosmochim. Acta* **43**, 1075 (1979).
9. W. S. Reeburgh, *Annu. Rev. Earth Planet. Sci.* **11**, 269 (1983).
10. P. P. E. Weaver and A. Kuijpers, *Nature (London)* **306**, 360 (1983).
11. W. B. Curry and G. P. Lohmann, *ibid.*, p. 577.
12. M. P. Bacon, *Isot. Geosci.* **2**, 97 (1984).
13. J. Thomson, T. R. S. Wilson, F. Culkin, D. J. Hydes, *Earth Planet. Sci. Lett.* **71**, 23 (1984).
14. We have considerably extended the numerical model used by Colley *et al.* (*1*) to include all the processes listed in the text. A steady-state analytical treatment (*2*) is used at each time step to calculate the instantaneous O_2 and NO_3^- pore-water profiles (Fig. 1 and Table 1). The fluxes of O_2 and NO_3^- to the reaction front are calculated from these profiles; the reductant (Fe^{2+} and Mn^{2+}) flux to the front (assumed to be constant) is subtracted to give a net oxidant flux. This is assumed to oxidize the sediment organic carbon according to the stoichiometry shown in Table 1; at each time step the resultant deepening of the front is calculated, and this new depth is used to recalculate the O_2 and NO_3^- profiles appropriate for the next time step. A listing of the model program Feline in structured BASIC is available from the authors.
15. Q. Huggett, personal communication.
16. R. J. Gibbs, *Geology* **9**, 77 (1981).
17. R. A. Berner, *Early Diagenesis: A Theoretical Approach* (Princeton Univ. Press, Princeton, NJ, 1969).

18. C. B. Officer, *Mar. Geol.* **46**, 261 (1982).
19. ——— and D. R. Lynch, *ibid.* **52**, 59 (1983).
20. J. Crank, *The Mathematics of Diffusion* (Clarendon, Oxford, 1956).
21. Y. H. Li and S. Gregory, *Geochim. Cosmochim. Acta* **38**, 703 (1974).
22. A. E. Bainbridge *et al.*, *GEOSECS [Geochemical Ocean Sections Study] Atlantic Expedition* (National Science Foundation–International Decade of Ocean Exploration, Washington, DC, 1980).

23. We thank W. S. Broecker for calling our attention to Richardson's thesis (*3*) and for providing us with a copy. This research has been carried out under contract for the United Kingdom Department of the Environment as part of its radioactive management research program. The results will be used in the formulation of government policy but, at this stage, do not necessarily represent that policy.

12 November 1985; accepted 11 March 1986

Sulfate and Nitrate Concentrations from a South Greenland Ice Core

P. A. MAYEWSKI, W. B. LYONS, M. J. SPENCER, M. TWICKLER, W. DANSGAARD, B. KOCI, C. I. DAVIDSON, R. E. HONRATH

An ice core in south Greenland covering the period 1869 to 1984 was analyzed for oxygen isotopes and chloride, nitrate, and sulfate concentrations. The data show that the "excess" (nonsea-salt) sulfate concentration has tripled since approximately 1900 to 1910 and the nitrate concentration has doubled since approximately 1955. The increases may be attributable to the deposition of these chemical species from air masses carrying North American and Eurasian anthropogenic emissions.

ONE OF THE MAJOR PROBLEMS associated with determining the effects of fossil fuel burning and acid deposition through time has been the lack of a reliable historic database for comparison with recent precipitation chemistry. Although it is believed that the hydrogen ion, sulfate, and nitrate concentrations in precipitation in the Northern Hemisphere have increased in the last few decades, detailed, continuous, long-term records in which there has been consistency in the way the samples have been collected, handled, and analyzed are lacking (*1*). Snow and ice cores collected from glaciers provide an opportunity to determine the chemistry of previously deposited precipitation and hence allow the production of reliable historic databases for areas remote from local anthropogenic influences.

In 1984, an electromechanically drilled core (*2*) was recovered from a site (65.01°N, 44.87°W, 2615 m above sea level) 40 km southwest and up-ice from a previously drilled site (Dye 3) in south Greenland. The site is believed to be free of any local contamination produced by Dye 3 (*3, 4*) and is located directly downwind from seasonally directed air masses that emanate from North America and Eurasia. It is ideal for the recovery of ice core records in general (*5*). Earlier chemical studies at Dye 3 by Herron (*6*) and Neftel *et al.* (*7*) have demonstrated the value of recovering records of sulfate and nitrate from south Greenland. However, these studies were based on multiyear averages of data over the last two millennia (*6*) or annual values since 1895 (*7*). Our record displays a total of 748 samples, equivalent to 6.5 samples per year, analyzed for chloride, "excess" sulfate (nonsea salt), nitrate, and oxygen isotopes (Fig. 1), as well as sodium (*8*), for the period 1869 to 1984 from a site unaffected by local contamination and hence valuable as a measure of North American and Eurasian anthropogenic activity.

All materials that contacted the samples were extensively tested (*8*) to ensure that the core was collected and processed without contamination. We used a cleaned polycarbonate subcorer to remove the outer 40 to 50% of core to guard against contamination potentially introduced during drilling. Blanks for the subcoring technique and the sample containers were <1.0 μg kg^{-1} for chloride and nitrate, <2.0 μg kg^{-1} for sulfate, and <2.7 μg kg^{-1} for sodium. All laboratory sample handling and processing before analysis was conducted in a cold room (−20°C). In the anion analyses we used a Dionex model 2010 ion chromatograph with an AS-4 column and 0.0021*M* $NaHCO_3$/0.0017*M* Na_2CO_3 eluent and a computer-driven autosampler. In the sodium analysis we used a stabilized-tempera-

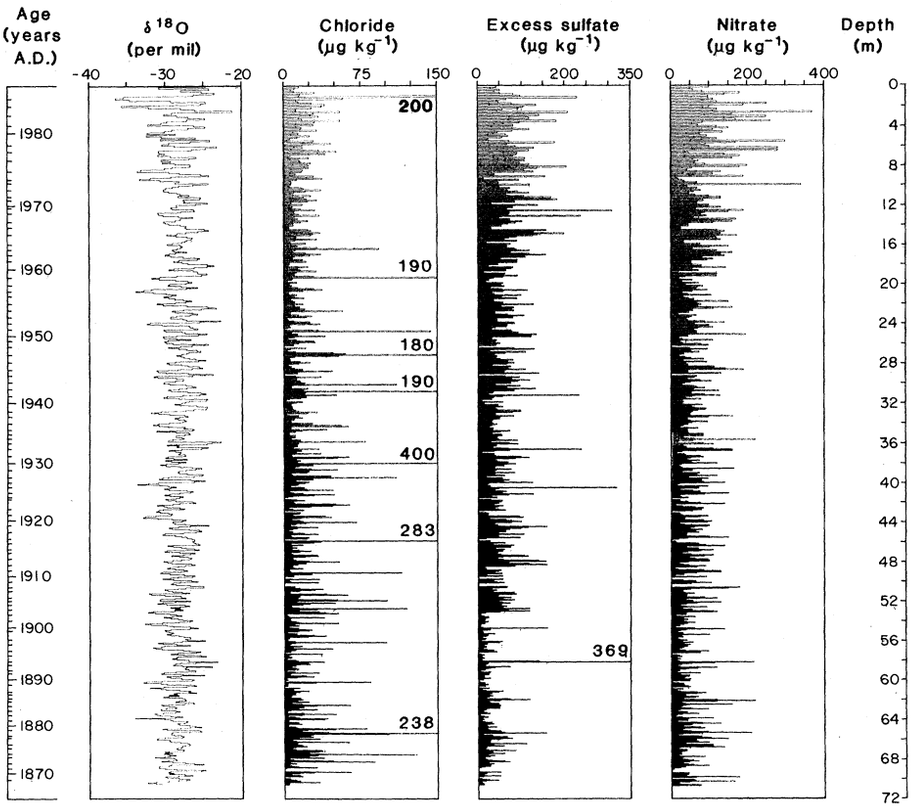

Fig. 1. Oxygen isotope, chloride, "excess" sulfate, and nitrate time series. Chloride and "excess" sulfate values that are off-scale appear as numbers. The time scale is compressed to accommodate annual layer compaction with depth.

P. A. Mayewski, W. B. Lyons, M. J. Spencer, M. Twickler, Glacier Research Group and Department of Earth Sciences, University of New Hampshire, Durham, NH 03824.
W. Dansgaard, Geophysical Isotope Laboratory, University of Copenhagen, Copenhagen, Denmark.
B. Koci, Polar Ice Coring Office, University of Nebraska, Lincoln, NE 68588.
C. I. Davidson and R. E. Honrath, Department of Civil Engineering, Carnegie-Mellon University, Pittsburgh, PA 15213.